Ultrafast Energy Transfer between Molecular Assemblies and Surface Plasmons in the Strong Coupling Regime

Maxim Sukharev,[†,*] Tamar Seideman,[‡] Robert J. Gordon,[§] Adi Salomon,[⊥,∥] and Yehiam Prior[∥]

[†]School of Letters and Sciences, Arizona State University, Mesa, Arizona 85212, United States, [‡]Department of Chemistry, Northwestern University, 2145 Sheridan Road, Evanston, Illinois 60201, United States, [§]Department of Chemistry, University of Illinois at Chicago, 845 West Taylor Street, Chicago, Illinois 60680, United States, [⊥]Department of Chemistry, Bar-Ilan University, Ramat-Gan, 52900, Israel, and [∥]Department of Chemical Physics, Weizmann Institute of Science, 76100 Rehovot, Israel

ABSTRACT The nonlinear optical dynamics of nanomaterials comprised of plasmons interacting with quantum emitters is investigated by a self-consistent model based on the coupled Maxwell—Liouville—von Neumann equations. It is shown that ultrashort resonant laser pulses significantly modify the optical properties of such hybrid systems. It is further demonstrated that the energy transfer between interacting molecules and plasmons occurs on a femtosecond time scale and can be controlled with both material and laser parameters.

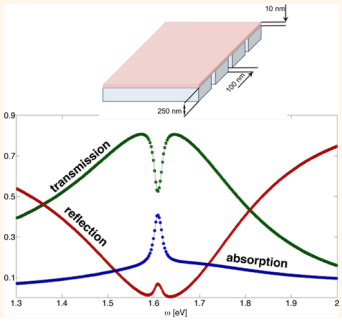

KEYWORDS: surface plasmon polaritons · hybrid materials · coherent control · transient spectroscopy

Noble metals, especially nanostructures, are well-known for their unique optical properties stemming from the phenomenon of surface plasmon-polariton (SPP) resonances.[1,2] This research area, known as nanoplasmonics, has grown rapidly in recent years, mainly because of potential applications of plasmonic materials.[3] Extreme concentration of electromagnetic (EM) radiation in nanoscale spatial regions was proposed[4] and implemented experimentally[5,6] as a method to achieve lasing. Other notable realizations of light EM field localization include surface-enhanced Raman spectroscopy[7] and tip-enhanced resonance microscopy.[8]

Among many exciting developments of nanoplasmonics lies the newly emerging research field of nanoscale optical molecular physics, which deals with ensembles of quantum particles optically coupled to nanomaterials[9] such as metal nanoparticles[10] (NP) and one- or two-dimensional periodic plasmonic arrays.[11−13] It has been shown, both theoretically[14−18] and experimentally,[19−21] that proper utilization of the optical properties of the metal nanostructures may lead to single atom/molecule optical trapping[14] as well as alignment and focusing. It is now possible[22] to control the geometry of nanomaterials (*e.g.*, NP shape, dimensions, and relative arrangement) with a precision on the order of 1 nm. This fine spatial control presents the key for successful manipulation of individual atoms and molecules.[15] The basis for this manipulation lies in the strong environmental[23] spatial dependence of the evanescent EM field, which generates large field gradients suitable for optical trapping, focusing, and alignment.[24] For example, it has been long known that local EM fields associated with metal NP dimers depend significantly on particle sizes and particle-to-particle distances.[25−27]

Despite considerable progress, our understanding of the optics of quantum media coupled to nanomaterials is still incomplete. Many recent works consider few quantum emitters driven by localized EM near-fields in plasmonic materials,[28−30] with only limited attempts to include collective effects,[31,32]

* Address correspondence to maxim.sukharev@asu.edu.

Received for review October 18, 2013 and accepted December 2, 2013.

Published online December 02, 2013
10.1021/nn4054528

which may play a critical role in the quantum optics of nanomaterials. Moreover, the optics of hybrid materials comprised of resonant microcavities and ensembles of quantum emitters (quantum dots[33−38] (QD), molecular aggregates,[39−41] nanocrystals,[42,43] and other dipoles[42,44]) have been a subject of extensive research in the past several years.[45] For example, it has been demonstrated[46] that the transmission and reflection spectra of a gold film are significantly modified by the deposition of a layer of J-aggregates on the film's surface. It was also shown experimentally[41] that SPP resonances have a large effect on the molecular electronic structure, leading to Rabi splitting of resonance peaks.[47] This phenomenon was proposed as a way of controlling the optics of hybrid materials with femtosecond laser pulses.[48] Furthermore, core−shell metal NPs with a shell comprised of optically active molecules have been recently studied experimentally,[49] demonstrating optimization of the coupling between J-aggregates and a localized SPP, which resulted in Rabi splitting as large as 200 meV. While experimental studies have clearly demonstrated the importance and unique optical properties of hybrid materials,[50] there remains a notable gap between the experimental progress and the status of theory and modeling of such systems.

The major parameters determining the strength of the interaction between molecular assemblies and SPP waves are the molecular concentration,[51,52] transition dipole moment,[52,53] and local field distribution enhanced by the nanostructure.[54] The strong coupling regime is reached when the field-induced Rabi splitting of the hybrid system surpasses all linewidths caused by the various damping rates.[55] Strong coupling manifests itself as an avoided crossing of the polariton modes when the plasmon frequency is varied, with a pronounced Rabi splitting that is a non-negligible fraction of the molecular transition frequency.[41,46,47,56−58] In this regime, energy exchange between the molecular and SPP modes is observed, giving rise to two new polariton eigenmodes. These states have mixed SPP-molecular properties that could be explored and utilized in various applications.[49] Most of the modeling of such systems was done with EM fields when SPP resonant conditions are used as an input for determining subsequent quantum dynamics of a molecular subsystem.[55] At high molecular concentrations, however, this approach is no longer valid because it fails to account for collective effects (*e.g.*, back action of the molecular dipole radiation on the local EM field, which in turn influences the molecules). Furthermore, it was shown recently that proper self-consistent modeling could explain the presence of an additional mode with mixed molecular-plasmon characteristics appearing in the transmission spectra of hybrid materials.[59]

RESULTS AND DISCUSSION

In the current work we utilize a self-consistent model based on the Maxwell−Liouville−von Neumann equations and examine the nonlinear dynamics of a hybrid nanomaterial comprised of a molecular layer optically coupled to a periodic array of sliver slits. We propose a simple method to simulate transient spectroscopy data for hybrid systems and show that in the strong coupling regime energy transfer occurs at the femtosecond time scale. Moreover, we demonstrate that the energy distribution can be controlled *via* laser and material parameters.

The interaction of EM radiation with molecular ensembles is treated using a semiclassical model based on the Maxwell−Liouville−von Neumann equations. The dynamics of the EM fields, $\vec{H}$ and $\vec{E}$, is governed by the classical Maxwell's equations,

$$\mu_0 \frac{\partial \vec{H}}{\partial t} = -\nabla \times \vec{E}, \qquad \varepsilon_0 \frac{\partial \vec{E}}{\partial t} = \nabla \times \vec{H} - \frac{\partial \vec{P}}{\partial t} \tag{1}$$

where μ_0 and ε_0 are the magnetic permeability and dielectric permittivity of free space, respectively. The macroscopic polarization $\vec{P}$ is calculated according to

$$\vec{P} = n_0 \langle \vec{d} \rangle = n_0 \mathrm{Tr}(\hat{\rho} \vec{d}) \tag{2}$$

where the density matrix $\hat{\rho}$ is the solution of the Liouville−von Neumann equation written in the Lindblad form,

$$\frac{d\hat{\rho}}{dt} = -(i/\hbar)[\hat{H}, \hat{\rho}] + \sum_n \frac{\gamma_n}{2} (2\hat{\sigma}_n^{(-)} \hat{\rho} \hat{\sigma}_n^{(+)} - \hat{\sigma}_n^{(+)} \hat{\sigma}_n^{(-)} \hat{\rho} - \hat{\rho} \hat{\sigma}_n^{(+)} \hat{\sigma}_n^{(-)}) \tag{3}$$

In eq 3, $-(i/\hbar)[\hat{H},\hat{\rho}]$ is the unitary part of the quantum evolution, $\hat{H}$ being the complete Hamiltonian, $\hat{\sigma}_n^{\mp}$ are the lowering and raising operators, and γ_n is the rate at which state $|n\rangle$ decays to the ground state $|1\rangle$ (typically referred to as a T_1 process). The dephasing rates (typically referred to as T_2 processes) are included in eq 3 in the off-diagonal terms. The relaxation processes are considered to be Markovian.

To include the back action of the molecules on the field at high molecular density, we introduce the Lorentz−Lorenz correction term for the local electric field in the form[60]

$$\vec{E}_{\mathrm{local}} = \vec{E} + \frac{1}{3\varepsilon_0} \vec{P} \tag{4}$$

It had been shown[61] that this local field correction eq 4 is valid also in case of EM wave propagation in dense, nonlinear media, a property we will need for the calculation of the transient absorption of light in hybrid nanomaterials.

In regions occupied by SPP-sustaining materials (*e.g.*, silver metal), we adopt the conventional Drude model for the dielectric constant of the metal,

$$\varepsilon(\omega) = \varepsilon_r - \frac{\Omega_p^2}{\omega^2 - i\Gamma\omega} \tag{5}$$

where ε_r is the high frequency limit of the dielectric constant, Ω_p is the bulk plasma frequency, and Γ is the

phenomenological damping rate for this specific metal. For the case considered here of silver at near visible frequencies, we use the values $\varepsilon_r = 8.926$, $\Omega_p = 1.760 \times 10^{16}$ rad/s, and $\Gamma = 3.084 \times 10^{14}$ s^{-1} derived from the work of Gray *et al.*[62]

The current density $\vec{J}$, which replaces the polarization current $\partial\vec{p}/\partial t$ in Ampere's law in eq 1, is evaluated according to[63]

$$\frac{\partial \vec{J}}{\partial t} = a\vec{J} + b\vec{E} \tag{6}$$

where $a = -\Gamma$ and $b = \varepsilon_0\Omega_p^2$.

We use here incident plane waves because we are mostly interested in targets that are much smaller than the incident wavelength. To ensure proper excitation we implement the total-field/scattered-field approach[63] with the following time dependence,

$$E_{inc} = E_0 f(t) \cos(\omega_{inc} t) \tag{7}$$

where the time envelope has the form $f(t) = \sin^2(\pi(t/\tau))$, and τ is the incident pulse duration. For probing transient effects, one typically uses "white light" with a flat spectrum over the spectral region of interest. We simulate a white light probe with a 0.36 fs long pulse, which produces an essentially flat spectrum for relevant energies between 1 and 4 eV. A probe amplitude of 1 V/m is used throughout this manuscript in order to lie in the weak field limit.

The key challenge in modeling nonlinear dynamics using a pump−probe pulse sequence is to disentangle signals caused by the strong pump from observations by the weak probe. When a system comprised of optically coupled emitters is excited by a strong pulse, it exhibits polarization oscillations lasting long after the pump is gone. Consequently, when the system is probed by a low intensity pulse, one observes an undesired high intensity signal at the pump frequency caused by induced polarization oscillations. Experimentally, such oscillations may be filtered out so as not to interfere with the probe in the far field. In simulations, these unwanted oscillations must be handled carefully because they may interfere with the signal produced by the probe.

Here we propose an efficient computational method to simulate transient spectroscopy experiments. The idea is illustrated in Figure 1. A high intensity pump drives a system under consideration during some time interval that we denote by $\Delta\tau$, at which time a probe pulse is applied. The Maxwell−Liouville−von Neumann equations are propagated in time and space with the driving pump up until the end of the interval $\Delta\tau$, at which time the density matrix elements are recorded at all grid points where the quantum medium is located. These data are used as initial conditions for simulation of the probe interaction with the sample. This method guarantees that undesired high amplitude oscillations are not included when one probes the system and that the probe does not alter the optical response of the system.

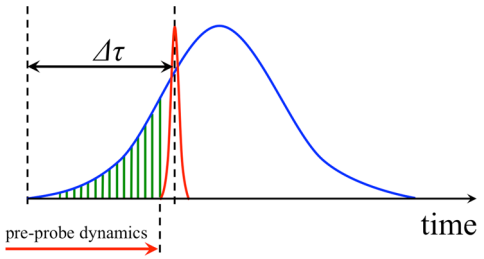

Figure 1. A high intensity pump (blue) interacts with the system under consideration (see text). At time $\Delta\tau$ after the start of the pump, a low intensity short probe (red) is applied, and its transmission (or absorption) is monitored.

Transient Spectroscopy of Molecular Nanolayers. We consider first a thin layer of interacting molecules, depicted schematically in the left inset of Figure 2. The layer is infinite in the *x* and *y* dimensions and finite in *z*. Each molecule in the layer is treated as a two-level system. The layer is subject to external plane wave excitation at normal incidence. The symmetry of the problem reduces the resulting system of coupled equations to the familiar one-dimensional Maxwell−Bloch equations.[64] With the assumption that all molecules are initially in the ground state, the one-photon absorption exhibits a broad resonance near the molecular transition, as shown in the main panel of Figure 2. This figure displays three absorption spectra, corresponding to different density regimes. One is calculated at a low molecular concentration (blue circles), showing a peak at the molecular transition frequency of 1.61 eV (the "noninteracting" molecules limit), a second corresponds to an intermediate concentration (green squares), and the third is a red-shifted (lower energy) spectrum for a high density sample (red diamonds), where the shift is caused by back action of the molecules on the field, as given by eq 4. The higher the molecular concentration, the greater the red shift, as expected. We also note that in our simulations the molecules are assumed to form a thin layer on the slit array without penetrating into the slits. Various experimental groups reported different setups with molecules not only covering a slit array but also filling in the slits.[48] Other experimental setups include quantum dots with the latter hardly penetrating the slits.[13] We performed several sets of test simulations, comparing linear spectra for empty slits with results obtained with slits filled with molecules. We find that even though absolute values of overall transmission/reflection/absorption and the positions of upper and lower polaritons vary slightly with slit conditions, the physics is qualitatively the same.

We next examine the nonlinear dynamics of such a system under strong pump excitation. As an illustrative example we consider a sequence of $n\pi$ pulses interacting with the molecular nanolayer (with no plasmonic substrate) under the assumption that all molecules

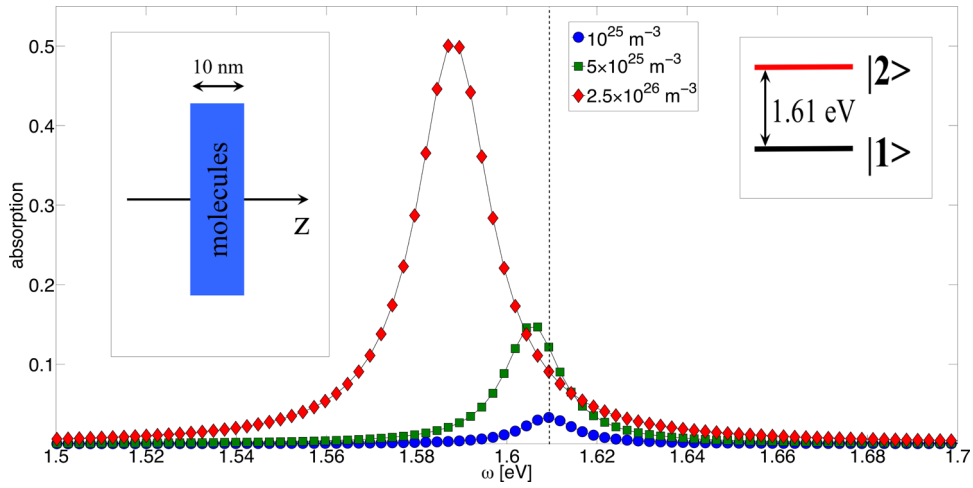

Figure 2. One-photon absorption for the 10 nm thick molecular layer depicted in the left inset as a function of the incident photon energy calculated at three molecular number densities: blue circles corresponding to 10^{25} m^{-3}, green squares for 5×10^{25} m^{-3}, and red diamonds for 2.5×10^{26} m^{-3}. The molecules are modeled as two-level emitters (right inset). The vertical dashed line shows the molecular transition energy of 1.61 eV. In these simulations the molecular transition dipole is 10 D, the radiationless lifetime of the excited state $|2\rangle$ is 1 ps, and the pure dephasing time is 100 fs.

are initially in the ground state. Following the numerical procedure discussed in the previous section, we calculate the instantaneous absorption of a probe pulse delayed relative to the pump excitation. Figure 3 shows the results for four different pump pulses, with n increasing from 1 to 4. As anticipated, the molecules undergo Rabi oscillations that depend on the pump pulse area. The absorption becomes negative (indicating gain) when the population is inverted. We also note three important observations: (1) it is more efficient to pump the system at the molecular transition energy, 1.61 eV, than at its red-shifted value of 1.59 eV (confirmed in a set of separate calculations not shown here); (2) the system undergoes transitions back to the ground state with the absorption centered at the red-shifted frequency because of strong mutual interaction between molecules at high concentrations; (3) the Rabi cycling is not complete, and each subsequent oscillation of the system from the ground state to the excited state is less pronounced, an effect that is attributed to decoherence.

Another important factor also contributes to the effect of incomplete Rabi cycling. Even though the thickness of the layer (10 nm) is much smaller than the incident wavelength (770 nm at 1.61 eV), the high molecular density causes the electric field inside the layer to be inhomogeneous; *i.e.* the local EM field decreases as one probes further within the molecular layer. This decrease results in a lower efficiency of the "nominal" $n\pi$-pulses. We note that this effect plays a significant role in hybrid systems, as we show in the next section.

Transient Spectroscopy of Periodic Hybrid Materials. The main goals of this paper are to examine the nonlinear optical dynamics in hybrid materials and to probe the influence of surface plasmons polaritons. Motivated in part by recent experimental work,[48,55] we consider a thin molecular layer deposited on top of a periodic array of slits in a silver film, as depicted in the inset of Figure 4a. In order to account for all possible polarizations of the EM field in the near-field zone,[65] individual molecules are treated as two-level emitters with a doubly degenerate excited state (see the inset of Figure 4b). The main panels of Figure 4a,b show the linear optical response of the hybrid system at two molecular concentrations. As in the case of a standalone molecular layer, we perform white-light transient spectroscopy simulations for normal incidence to compute the transmission coefficient, T, and the reflection coefficient, R. Since our simulations are performed in the weak probe (linear) regime, one may also calculate the absorption using energy conservation,

$$A = 1 - T - R \tag{8}$$

Figure 4a shows all three coefficients at low molecular concentration calculated before the pump arrives ($\Delta\tau = 0$). One can clearly see the Rabi splitting in both transmission and reflection. Maxima in transmission correspond precisely to minima in reflection, indicating the energies of the hybrid system, *i.e.*, the upper and lower polaritons. Absorption, on the other hand, has a single narrow resonance with a full width at half-maximum corresponding to the energy of the Rabi splitting. (For the given set of parameters, the Rabi splitting is 75 meV). It should be noted that the observed splitting in both transmission and reflection coefficients is indeed the Rabi splitting and is not caused by simple molecular absorption. One may verify this explanation by calculating the effect of varying either the angle of incidence or the periodicity of the slit array on the energies of the upper and lower polaritons.[59] These calculations show strong

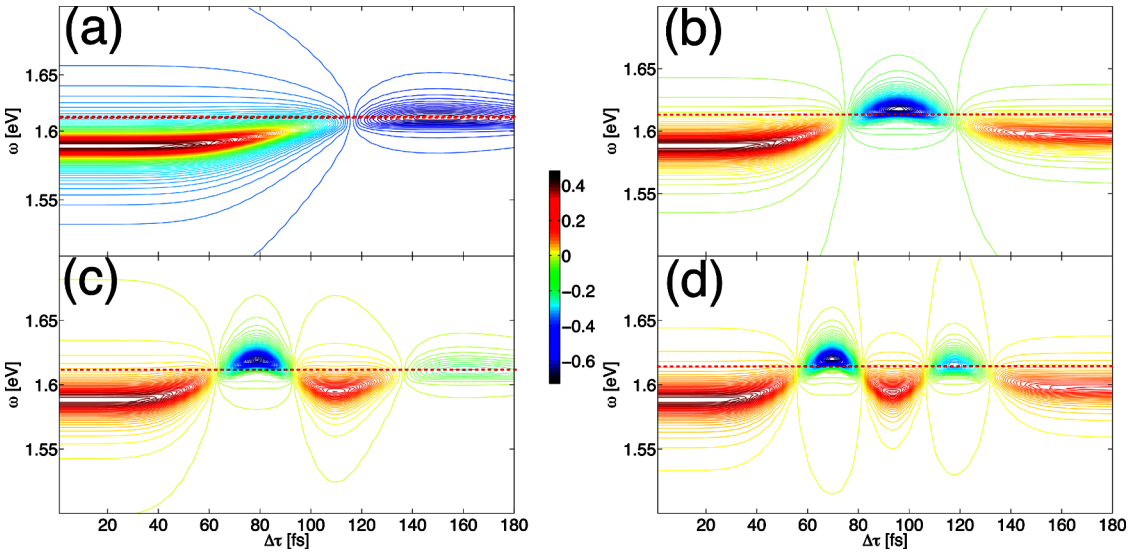

Figure 3. Transient absorption spectra of the pure molecular system as a function of the pump−probe delay (horizontal axis) and the incident photon energy (vertical axis) evaluated for 180 fs pump pulses. The horizontal dashed red line in each panel is at the molecular transition energy, 1.61 eV. Panel (a) shows the spectrum for a π-pulse ($E_0 = 2.075 \times 10^8$ V/m), panel (b) shows the data for a 2π-pulse ($E_0 = 4.150 \times 10^8$ V/m), panel (c) shows results for a 3π-pulse ($E_0 = 6.225 \times 10^8$ V/m), and panel (d) is for a 4π-pulse ($E_0 = 8.300 \times 10^8$ V/m). In all cases the pump frequency is resonant with the molecular transition energy. Other parameters are the same as in Figure 2. A pump−probe delay of 0 fs corresponds to the probe applied at a time when the pump is still off (*i.e.*, at the beginning of the leading edge of the pump; see Figure 1 for details).

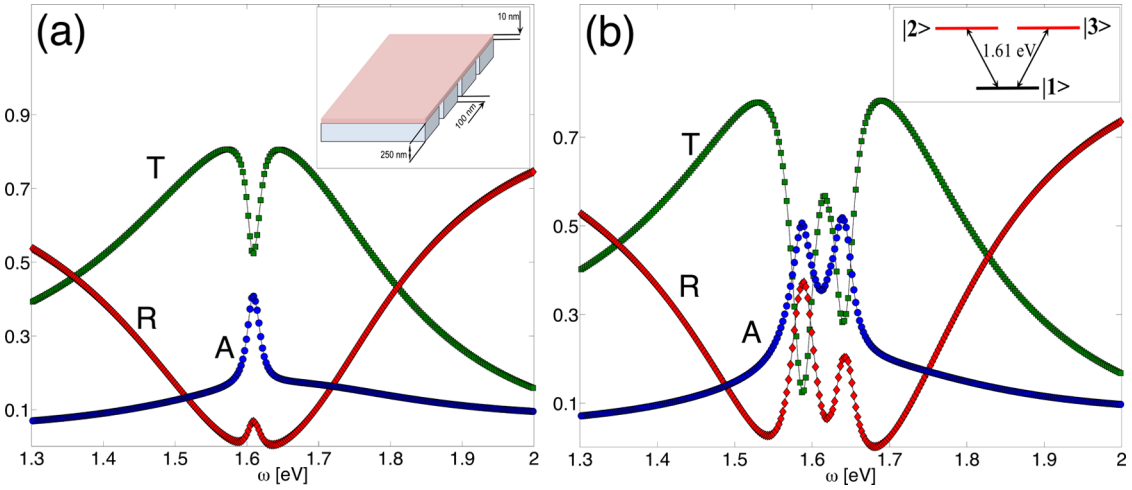

Figure 4. Extinction spectra of the hybrid material depicted in the inset of panel (a). Both panels show absorption, *A*, (blue circles), transmission, *T*, (green squares), and reflection, *R*, (red diamonds) as functions of the incident photon energy. Individual molecules are considered as two-level emitters with a doubly degenerate excited state, as shown in the inset of panel (b). Panel (a) shows spectra at a low molecular number density of 3×10^{25} m^{-3}. Panel (b) shows the results of simulations at a higher density of 2.5×10^{26} m^{-3}. The slit array period is 410 nm. The other parameters are as in Figure 2.

dispersion along with an avoided crossing, a clear indication of strong coupling between molecular excitons and plasmons.

Figure 4b presents results of simulations at higher molecular density, clearly showing a collective molecular-plasmon mode[59] at 1.61 eV. This energy corresponds to a maximum in *T* and a minimum in *R*. Note that absorption now has two peaks, which match the positions of the minima of *T* and maxima of *R*. Anticipating comparison with experiments, we monitor the nonlinear changes in the reflection spectra rather than the transmission. These changes may be expressed as the ratio

$$\Delta R(\Delta\tau, \omega) = \frac{R(\Delta\tau, \omega) - R(0, \omega)}{R(0, \omega)} \quad (9)$$

where $R(0,\omega)$ is the unperturbed reflection in the absence of the pump.

Figure 5a shows the transient spectrum for a 15 fs pump resonant with the molecular transition frequency at 1.61 eV. The calculated spectra exhibit pronounced oscillations centered about three distinct

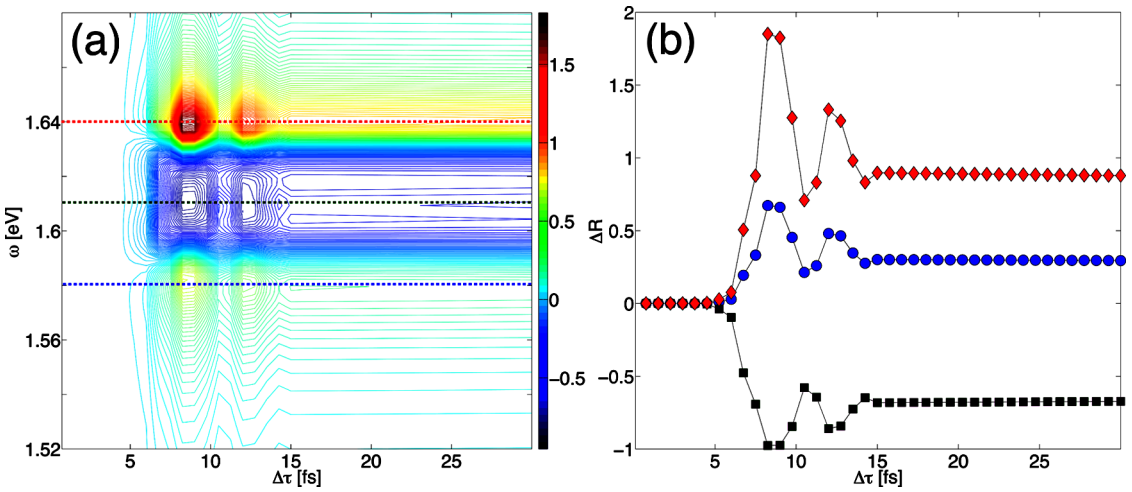

Figure 5. Transient spectroscopy calculations for a 15 fs pump pulse with a peak amplitude of 4×10^9 V/m centered at the molecular transition energy of 1.61 eV. Panel (a) shows the change in reflection ΔR (see eq 9) as a function of the pump−probe delay and incident photon energy. Panel (b) depicts one-dimensional cuts of ΔR at three energies: blue circles are for the lower polariton at 1.572 eV (this energy is also indicated in panel (a) as a horizontal blue dashed line), red diamonds are for the upper polariton at 1.647 eV (also shown in panel (a) as a horizontal red dashed line), and black squares are for the molecular line at 1.61 eV (shown in panel (a) as a horizontal black dashed line). The molecular number density is 3×10^{25} m^{-3} (see Figure 4a), and the period of the slit array is 410 nm. The other parameters are as in Figure 2.

energies, two of which correspond to the upper and lower polaritons (the minima of the unperturbed reflection, see Figure 4), while the third is at the molecular transition energy. This result is consistent with recent experimental observations;[55] namely that the reflection is increased during the pump at the energies of the upper and lower polaritons. One should also note the asymmetry in the reflection signal: the upper polariton is significantly more enhanced than the lower one. This effect is most likely due to the fact that the unperturbed reflection (Figure 4a) is already asymmetric, with the molecular transition energy slightly offset toward the upper polariton. Another observation worth noting is that reflection is suppressed at 1.61 eV ($\Delta R < 0$), whereas transmission is enhanced. The molecules that mostly affect both transmission and reflection are located in close proximity to the slits. Resonant excitation of these spatial regions results in strong coupling of molecular excitons and SPP modes, thereby suppressing reflection and enhancing transmission, a phenomenon similar to extraordinary optical transmission.

To demonstrate that the observed changes are caused by energy transfer between the upper/lower polaritons and the molecular layer, we plot ΔR in Figure 5b at three energies as a function of the pump−probe delay. The oscillation period is 3.75 fs. Interestingly, simulations performed at higher molecular concentrations or different array spacings show that these factors have a very minimal effect on the oscillation period, which is fully determined by the local electric field amplitude and the strength of the molecular dipole. We note that hybrid systems exhibit an additional mixed plasmon-molecular mode at high molecular concentrations, as was shown recently in ref 59. Nonlinear dynamics at such concentrations has Rabi oscillations with periods nearly identical to those obtained at low densities and a splitting that varies as the square root of the molecular density, but the energy distribution near the molecular line is more complex. Understanding of such distributions is one of the subjects of our future research.

We also performed calculations using off-resonant pump excitation, as in ref 55. The data obtained for the off-resonant case shows the same behavior: ultrafast energy oscillations between the upper/lower polaritons and the molecules.

Next we proceed to examine the influence of the pump peak amplitude on the nonlinear dynamics. In order to observe many Rabi oscillations cycles but still maintain a moderate incident peak amplitude, we use a pump pulse with a duration of 30 fs. Figure 6 presents ΔR at two peak amplitudes at the energy of the upper polariton as a function of the time delay. As expected, the Rabi oscillation period decreases with the increase of the pump amplitude. The average oscillation period at 4×10^9 V/m is ~3 fs, whereas the calculations for 2×10^9 V/m indicate a period of ~6 fs. These calculations display at least two surprising features. First, the Rabi period is not constant, but rather decreases with time (detailed data not shown). (We note that this variation was also observed in ref 55.) Second, the Rabi period obtained from the simulations (the average oscillation period at 2×10^9 V/m is 6.9 fs) is smaller than the one obtained assuming a simple two-level atom in the same laser field (17 fs at 2×10^9 V/m).[64]

It is incorrect to use the peak Rabi frequency to estimate the oscillation period of the population for a two-level emitter exposed to short pulse excitation.

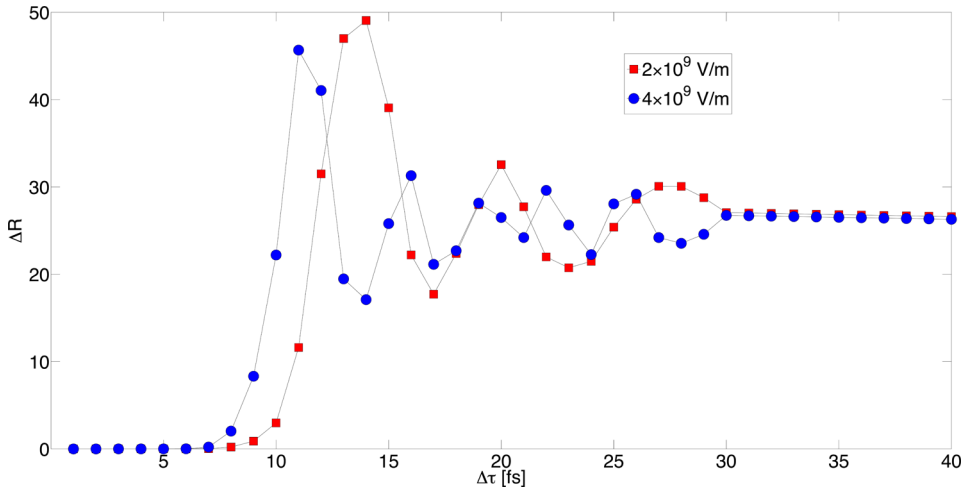

Figure 6. The change in reflection ΔR as a function of the pump−probe delay at the upper polariton energy for two pump amplitudes: red squares are for 2×10^9 V/m (peak amplitude) showing an oscillation period of 6 fs, and blue circles are for 4×10^9 V/m with a period of 3 fs. The pump is resonant with the molecular transition energy (1.61 eV), and its duration is 30 fs. The other parameters are as in the previous figures.

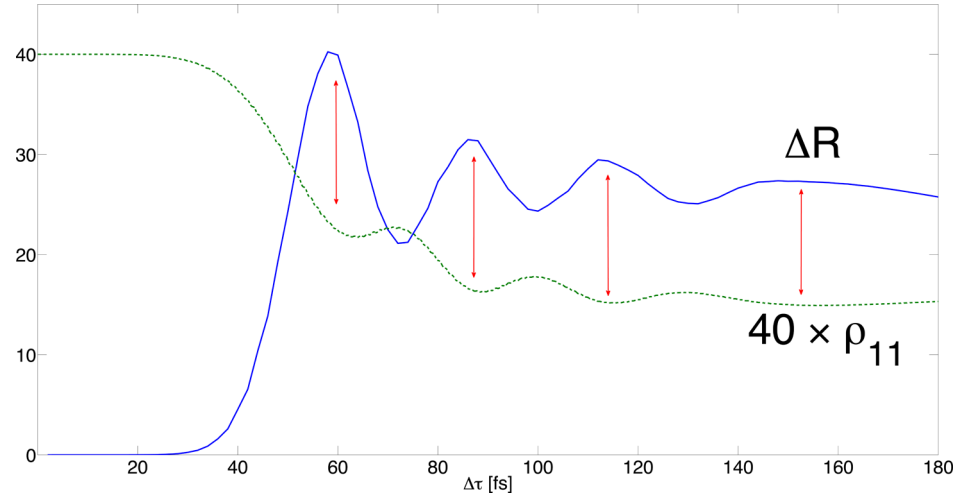

Figure 7. Nonlinear dynamics during a 180 fs pump. The blue solid curve shows ΔR as a function of the pump−probe delay at the upper polariton energy. The dashed green curve presents the ensemble-averaged ground state population of the molecular system. (The population ρ_{11} is multiplied by 40 for clarity). Vertical red arrows indicate direct correspondence between oscillations in reflection and the ground state population. The pump amplitude is 4.3×10^8 V/m. The incident frequency is at the molecular transition energy of 1.61 eV. The other parameters are as in Figure 2.

Rather, one has to take carefully into account the laser pulse envelope, calculating the pump pulse area as

$$S = \frac{d_0 E_0}{\hbar} \int f(t)\, dt \qquad (10)$$

where d_0 is the transition dipole moment of the quantum emitter. For observations after the end of the pulse, the integral should be over the entire pulse envelope, whereas for measurements during the pulse, the integral should be taken up to the time of observation by the probe. For an incident source of the form in eq 7, the pulse area becomes

$$S = \frac{d_0 E_0 \tau_{\text{pump}}}{2\hbar} \qquad (11)$$

For example, for a 30 fs pump with an amplitude of 2×10^9 V/m and the molecular parameters in Figure 2, we have $S = 1.74\pi$. Consequently, a two-level emitter exposed to such an excitation undergoes less than one Rabi cycle. (The population remaining in the ground state is 0.74 after the pump; *i.e.* the emitter is excited and then partially de-excited). Simple calculations performed for a single two-level emitter agree perfectly with eq 11.

If we now apply this simple model to estimate how many Rabi cycles the hybrid material undergoes, we find that the number of cycles predicted by eq 11 is always smaller than the actual number computed from the complete set of Maxwell−Liouville−von Neumann equations. The only parameter that is different in the

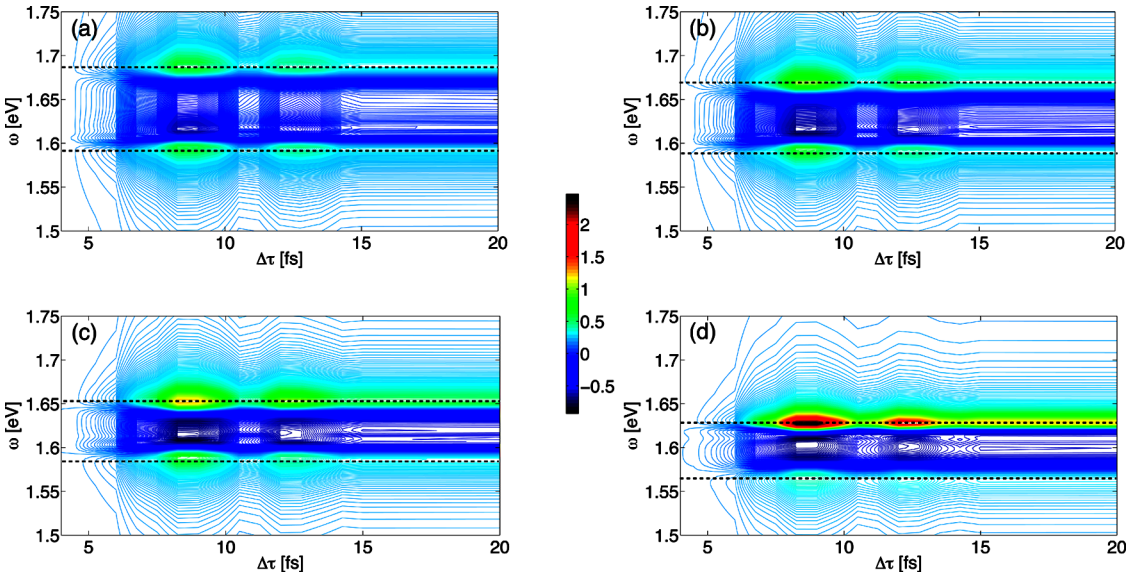

Figure 8. Change in reflectivity, ΔR, as a function of the pump−probe delay and incident photon energy for different slit array periods: (a) 350, (b) 370, (c) 390, and (d) 440 nm. The two horizontal dashed lines in each panel indicate the energy positions of the upper and lower polaritons. The pump pulse duration is 15 fs, the peak amplitude is 4×10^9 V/m, the incident frequency is at the molecular line of 1.61 eV, and the molecular number density is 3×10^{25} m^{-3}. Other parameters are as in Figure 2.

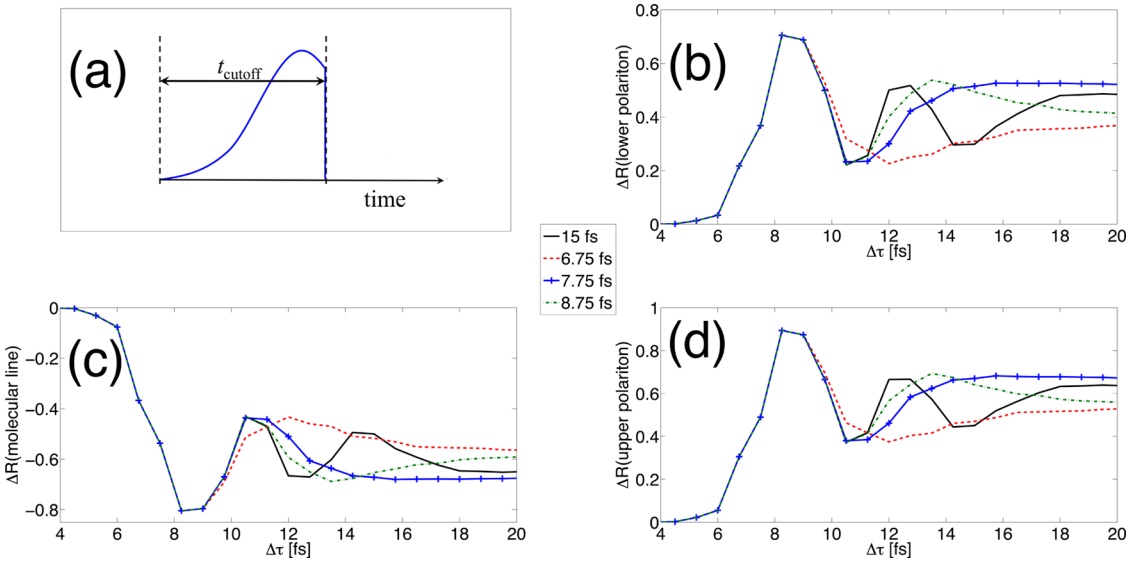

Figure 9. Effect of the laser pulse shape on the change in reflectivity. Panel (a) illustrates the abrupt cutoff of the pump pulse and application of the probe pulse at time t_{cutoff}, which is used as a control parameter. Panels (b)−(d) show ΔR as a function of the pump−probe delay at different photon energies. Black solid curves show results for a nontruncated pump, red dashed curves show data for t_{cutoff} = 6.75 fs, blue solid curves with crosses are for t_{cutoff} = 7.75 fs, and green dash-dotted lines are for t_{cutoff} = 8.75 fs. Panel (b) shows ΔR at the lower polariton energy of 1.59 eV, panel (c) shows ΔR at the molecular transition energy of 1.61 eV, and panel (d) presents ΔR at the upper polariton energy of 1.67 eV. Simulations are performed for a slit array with a period of 370 nm. The total pump pulse duration is 15 fs, the peak amplitude is 4×10^9 V/m, the incident frequency is at the molecular line of 1.61 eV, and the molecular number density is 3×10^{25} m^{-3}. Other parameters are as in Figure 2.

complete model is the local electric field, which differs from its incident value in the near-field zone because of SPPs. The local field enhancement hence plays a crucial role in determining how rapidly energy oscillates in hybrid materials.

Simulations using longer pump pulses reveal a direct connection between the excitation dynamics and transient spectra of the system, as illustrated in Figure 7. There is a clear correspondence between oscillations of the ground state population and changes in reflection induced by the pump. (A similar correlation was found for ΔT.) We conclude, therefore, that the observed oscillations in the transient spectra are due to quantum transitions between ground and excited states in individual molecules.

We conclude this section by examining the role of dephasing in hybrid materials. This property is greatly affected by the inhomogeneous electric field due to SPPs, as is evident from Figure 7. One of the causes of the fast decay of Rabi oscillations (in addition to pure decoherence and relaxation caused by interaction with the metallic system, which is explicitly included in the model) is spatially dependent excitation of the molecular layer, resulting from the strong gradient of the electric field induced mainly by surface plasmons. Different parts of the molecular ensemble therefore experience different local fields. This effect in turn changes the plasmon dynamics, influencing not only the amplitude of Rabi oscillations but also the Rabi period. It should be noted that the molecular layer influences the near-field *via* the polarization current, which results in even faster dephasing. Simulations with a thicker molecular layer confirm the aforementioned conclusion; *i.e.*, the Rabi oscillations decay significantly faster when a 10 nm thick molecular layer is replaced by a layer with a thickness of 50 nm.

Control of the Energy Distribution in Hybrid Materials. The asymmetry of the energy distribution between the upper and lower polaritons is due to the relative position of the molecular transition energy with respect to the SPP resonance. Such a property of hybrid systems, along with the intriguing experimental possibilities of controlling the structural parameters of plasmonic nanomaterials, call for possible control of the plasmon energy distribution. One may shift the plasmon resonances by changing various material parameters, such as film thickness, period, slit width, *etc*. Figure 8 illustrates this idea by examining transient spectra of the hybrid system for different slit periods.

The possibility of such control is due to the strong dispersion of the upper and lower polaritons in hybrid systems.[41] As the plasmon resonance sweeps through the molecular line (for varying slit periodicity), the mixed plasmon-molecular hybrid modes drastically change their positions. The energy is more equally distributed among the upper and lower polaritons at shorter periods, as evident from Figure 8. One may also envision control by changing the angle of incidence, as this parameter changes the in-plane wave vector, which in turn would change the energy distribution in a fashion similar to varying the array period.[66]

A more intriguing control possibility is to utilize the full machinery of the incident laser radiation. To demonstrate how the characteristics of the laser pulse affect the polariton energy distribution, we performed a series of pump−probe simulations varying the time envelop of the pump by turning it off "suddenly", namely, on a time-scale short compared to the natural system time-scales. Figure 9a depicts schematically a control pump with time duration t_{cutoff}. Figure 9b−d shows the results of simulations for an array of slits with a period of 370 nm. By controlling t_{cutoff} one may control the number and phase of the Rabi cycles and, as a result, the plasmon energy distribution as well. We can envision simultaneously varying both the time envelope of the pump and its incident angle. The former would control which mode the energy of the system goes to, while the latter manipulates the distribution of energy between the upper and lower polaritons.

An interesting observation is "Free Induction Decay" type oscillations at times $t > t_{cutoff}$, a result of the coherent superposition of the polariton population prepared by the pump pulse before its abrupt termination at t_{cutoff}, as seen in Figure 9. Note that for very short times after the cutoff, the dynamics of ΔR barely differs from the corresponding dynamics with the pulse on.

CONCLUSION

Using a self-consistent model of the coupled Maxwell−Liouville−von Neumann equations, we scrutinized the nonlinear dynamics of nanomaterials comprised of interacting quantum emitters and plasmons. We showed that ultrashort resonant laser pulses significantly modify the optical properties of such hybrid systems. It was demonstrated that energy transfer between the molecular layer and surface plasmons occurs on a femtosecond time scale. This energy transfer may be controlled by altering the material and/or laser parameters. When an intense resonant laser pulse excites a quantum medium coupled to a plasmonic material, the induced spatial distribution of the population of the excited quantum states depends strongly on the incident wavelength and the geometry of the plasmonic material, among other optical and material parameters. If the peak amplitude of the incident field is sufficiently high, the quantum emitters may be driven through one or more Rabi cycles, so that at the end of the pulse they will be in a predetermined quantum superposition of molecular states. The final superposition depends on the local EM field, which is subject to external control (*e.g.*, through variation of the distance from the plasmonic material).

Within the lifetime of the excited states, which may be relatively long for specific systems, the quantum system is being modified by the laser pulse so that its macroscopic refractive index is changed. It should be emphasized that this modification is spatially dependent, with a characteristic length scale much smaller than the incident wavelength. We note that the close proximity of plasmonic materials modifies the refractive index in a spatially dependent manner due to the strongly inhomogeneous near-fields, leading to a modified, highly anisotropic refractive index. One may then probe the system with a low intensity pulse to measure the new refractive index.

Our results suggest a wide variety of future research opportunities, ranging from control of the competition between charge transport and energy transfer, a hurdle in control of light-triggered molecular conduction junctions, to modification of the relationship between light enhancement and excited state quenching, the main handicap of plasmon enhanced spectroscopies.

METHODS

The resulting system of partial differential eqs 1, 3, 6 is discretized in space and time using the finite-difference time-domain method.[63] Maxwell's equations, along with the Liouville–von Neumann equation, are propagated self-consistently in time at every grid point driven by the local electric field, using the weakly coupled method outlined in refs 65, 67. For all calculations, irrespective of the dimensionality, numerical convergence is achieved at the spatial resolution of $\delta x = 1$ nm and a time step of $\delta t = \delta x/(2c) = 1.7 \times 10^{-3}$ fs, where c is the speed of light in vacuum. To simulate semi-infinite spatial systems we implement the convolutional perfectly matched layers (CPML) absorbing boundaries.[68] In simulations of molecular aggregates coupled to plasmonic materials, we used the following set of parameters: the molecular transition dipole is 10 D, the radiationless lifetime of the molecular excited state is 1 ps, and the pure dephasing time is 100 fs.

Conflict of Interest: The authors declare no competing financial interest.

Acknowledgment. M.S. is grateful to the Air Force Office of Scientific Research that partially supported this research *via* Summer Faculty Research Fellowship 2013. T.S. thanks the NSF (Grant No. CHE-1012207/001 and Grant No. DMR-1121262) for support. R.J.G. thanks the NSF for support under Grant No. CHE-0848198. Y.P. and A.S. acknowledge support by the Israel Science Foundation Grant No. 1242/12.

REFERENCES AND NOTES

1. Kreibig, U.; Vollmer, M. *Optical Properties of Metal Clusters*; Springer: Berlin, 1995.
2. Raether, H. Surface-Plasmons on Smooth and Rough Surfaces and on Gratings. *Springer Tracts Mod. Phys.* **1988**, *111*, 1–133.
3. Gramotnev, D. K.; Bozhevolnyi, S. I. Plasmonics Beyond the Diffraction Limit. *Nat. Photonics* **2010**, *4*, 83–91.
4. Bergman, D. J.; Stockman, M. I. Surface Plasmon Amplification by Stimulated Emission of Radiation: Quantum Generation of Coherent Surface Plasmons in Nanosystems. *Phys. Rev. Lett.* **2003**, *90*, 027402.
5. Zheludev, N. I.; Prosvirnin, S. L.; Papasimakis, N.; Fedotov, V. A. Lasing Spaser. *Nat. Photonics* **2008**, *2*, 351–354.
6. Zhang, X.; Oulton, R. F.; Sorger, V. J.; Zentgraf, T.; Ma, R. M.; Gladden, C.; Dai, L.; Bartal, G. Plasmon Lasers at Deep Subwavelength Scale. *Nature* **2009**, *461*, 629–632.
7. Le Ru, E. C.; Etchegoin, P. G. *Principles of Surface-Enhanced Raman Spectroscopy and Related Plasmonic Effects*; Elsevier Science & Technology Books: San Diego, 2008.
8. Hartschuh, A. Tip-Enhanced Near-Field Optical Microscopy. *Angew. Chem., Int. Ed.* **2008**, *47*, 8178–8191.
9. Chang, D. E.; Sorensen, A. S.; Hemmer, P. R.; Lukin, M. D. Quantum Optics with Surface Plasmons. *Phys. Rev. Lett.* **2006**, *97*, 053002.
10. Dulkeith, E.; Morteani, A. C.; Niedereichholz, T.; Klar, T. A.; Feldmann, J.; Levi, S. A.; van Veggel, F. C. J. M.; Reinhoudt, D. N.; Moller, M.; Gittins, D. I. Fluorescence Quenching of Dye Molecules Near Gold Nanoparticles: Radiative and Nonradiative Effects. *Phys. Rev. Lett.* **2002**, *89*, 203002.
11. Dintinger, J.; Klein, S.; Bustos, F.; Barnes, W. L.; Ebbesen, T. W. Strong Coupling Between Surface Plasmon-Polaritons and Organic Molecules in Subwavelength Hole Array. *Phys. Rev. B* **2005**, *71*, 035424.
12. Vasa, P.; Pomraenke, R.; Schwieger, S.; Mazur, Y. I.; Kunets, V.; Srinivasan, P.; Johnson, E.; Kihm, J. E.; Kim, D. S.; Runge, E.; *et al.* Coherent Exciton-Surface-Plasmon-Polariton Interaction in Hybrid Metal-Semiconductor Nanostructures. *Phys. Rev. Lett.* **2008**, *101*, 116801.
13. Livneh, N.; Strauss, A.; Schwarz, I.; Rosenberg, I.; Zimran, A.; Yochelis, S.; Chen, G.; Banin, U.; Paltiel, Y.; Rapaport, R. Highly Directional Emission and Photon Beaming from Nanocrystal Quantum Dots Embedded in Metallic Nanoslit Arrays. *Nano Lett.* **2013**, *11*, 1630–1653.
14. Garcia-Segundo, C.; Yan, H.; Zhan, M. S. Atom Trap with Surface Plasmon and Evanescent Field. *Phys. Rev. A* **2007**, *75*, 030902.
15. Chang, D. E.; Thompson, J. D.; Park, H.; Vuletic, V.; Zibrov, A. S.; Zoller, P.; Lukin, M. D. Trapping and Manipulation of Isolated Atoms Using Nanoscale Plasmonic Structures. *Phys. Rev. Lett.* **2009**, *103*, 123004.
16. Yannopapas, V.; Vitanov, N. V. All-optical Nanotraps for Atoms atop Flat Metamaterial Lenses: a Theoretical Study. *J. Phys.: Condens. Matter* **2009**, *21*, 245901.
17. Arun, R.; Cohen, O.; Averbukh, I. S. Atom Lithography with Near-Resonant Standing Waves. *Phys. Rev. A* **2010**, *81*, 063809.
18. Schmidt, R.; Chormaic, S. N.; Minogin, V. G. van der Waals Interaction of a Neutral Atom with the Surface of a Metal or Dielectric Nanosphere. *J. Phys. B: At., Mol. Opt. Phys.* **2011**, *44*, 015004.
19. Vetsch, E.; Reitz, D.; Sague, G.; Schmidt, R.; Dawkins, S. T.; Rauschenbeutel, A. Optical Interface Created by Laser-Cooled Atoms Trapped in the Evanescent Field Surrounding an Optical Nanofiber. *Phys. Rev. Lett.* **2010**, *104*, 203603.
20. Zhan, M. S.; Xu, P.; He, X. D.; Wang, J. Trapping a Single Atom in a Blue Detuned Optical Bottle Beam Trap. *Opt. Lett.* **2010**, *35*, 2164–2166.
21. Kimble, H. J.; Alton, D. J.; Stern, N. P.; Aoki, T.; Lee, H.; Ostby, E.; Vahala, K. J. Strong Interactions of Single Atoms and Photons Near a Dielectric Boundary. *Nat. Phys.* **2011**, *7*, 159–165.
22. Sun, Y. G.; Xia, Y. N. Shape-Controlled Synthesis of Gold and Silver Nanoparticles. *Science* **2002**, *298*, 2176–2179.
23. Sukharev, M.; Seideman, T. Coherent Control of Light Propagation *via* Nanoparticle Arrays. *J. Phys. B: At., Mol. Opt. Phys.* **2007**, *40*, S283–S298.
24. Artamonov, M.; Seideman, T. Molecular Focusing and Alignment with Plasmon Fields. *Nano Lett.* **2010**, *10*, 4908–4912.
25. Romero, I.; Aizpurua, J.; Bryant, G. W.; de Abajo, F. J. G. Plasmons in Nearly Touching Metallic Nanoparticles: Singular Response in the Limit of Touching Dimers. *Opt. Express* **2006**, *14*, 9988–9999.
26. McMahon, J. M.; Gray, S. K.; Schatz, G. C. Fundamental Behavior of Electric Field Enhancements in the Gaps Between Closely Spaced Nanostructures. *Phys. Rev. B* **2011**, *83*, 115428.
27. Salomon, A.; Zielinski, M.; Kolkowski, R.; Zyss, J.; Prior, Y. Size and Shape Resonances in Second Harmonic Generation from Silver Nanocavities. *J. Phys. Chem. C* **2013**, *117*, 22377–22382.
28. Lopata, K.; Neuhauser, D. Molecular Nanopolaritonics: Cross Manipulation of Near-Field Plasmons and Molecules. I. Theory and Application to Junction Control. *J. Chem. Phys.* **2007**, *127*, 154715.
29. Lopata, K.; Neuhauser, D. Multiscale Maxwell-Schrodinger Modeling: A Split Field Finite-Difference Time-Domain Approach to Molecular Nanopolaritonics. *J. Chem. Phys.* **2009**, *130*, 104707.
30. Lopata, K.; Neuhauser, D. Nonlinear Nanopolaritonics: Finite-Difference Time-Domain Maxwell-Schroumldinger Simulation of Molecule-Assisted Plasmon Transfer. *J. Chem. Phys.* **2009**, *131*, 014701.

31. Fratalocchi, A.; Conti, C.; Ruocco, G. Three-Dimensional *Ab Initio* Investigation of Light-Matter Interaction in Mie Lasers. *Phys. Rev. A* **2008**, *78*, 013806.
32. Choquette, J. J.; Marzlin, K. P.; Sanders, B. C. Superradiance, Subradiance, and Suppressed Superradiance of Dipoles Near a Metal Interface. *Phys. Rev. A* **2010**, *82*, 023827.
33. Panzarini, G.; Andreani, L. C.; Armitage, A.; Baxter, D.; Skolnick, M. S.; Astratov, V. N.; Roberts, J. S.; Kavokin, A. V.; Vladimirova, M. R.; Kaliteevski, M. A. Cavity-Polariton Dispersion and Dolarization Splitting in Single and Coupled Semiconductor Microcavities. *Phys. Solid State* **1999**, *41*, 1223–1238.
34. Reithmaier, J. P.; Sek, G.; Loffler, A.; Hofmann, C.; Kuhn, S.; Reitzenstein, S.; Keldysh, L. V.; Kulakovskii, V. D.; Reinecke, T. L.; Forchel, A. Strong Coupling in a Single Quantum Dot-Semiconductor Microcavity System. *Nature* **2004**, *432*, 197–200.
35. Agranovich, V. M.; La Rocca, G. C. Electronic Excitations in Organic Microcavities with Strong Light-Matter Coupling. *Solid State Commun.* **2005**, *135*, 544–553.
36. Khitrova, G.; Gibbs, H. M.; Kira, M.; Koch, S. W.; Scherer, A. Vacuum Rabi Splitting in Semiconductors. *Nat. Phys.* **2006**, *2*, 81–90.
37. Chen, G. Y.; Chen, Y. N.; Chuu, D. S.; Brandes, T. Quantum-Dot Exciton Dynamics with a Surface Plasmon: Band-Edge Quantum Optics. *Phys. Rev. A* **2009**, *79*, 033815.
38. Toropov, A. A.; Shubina, T. V.; Jmerik, V. N.; Ivanov, S. V.; Ogawa, Y.; Minami, F. Optically Enhanced Emission of Localized Excitons in In(x)Ga(1-x)N Films by Coupling to Plasmons in a Gold Nanoparticle. *Phys. Rev. Lett.* **2009**, *103*, 037403.
39. Bellessa, J.; Bonnand, C.; Plenet, J. C.; Mugnier, J. Strong Coupling Between Surface Plasmons and Excitons in an Organic Semiconductor. *Phys. Rev. Lett.* **2004**, *93*, 036404.
40. Cade, N. I.; Ritman-Meer, T.; Richards, D. Strong Coupling of Localized Plasmons and Molecular Excitons in Nanostructured Silver Films. *Phys. Rev. B* **2009**, *79*, 241404.
41. Salomon, A.; Genet, C.; Ebbesen, T. W. Molecule-Light Complex: Dynamics of Hybrid Molecule-Surface Plasmon States. *Angew. Chem., Int. Ed.* **2009**, *48*, 8748–8751.
42. Gomez, D. E.; Vernon, K. C.; Mulvaney, P.; Davis, T. J. Surface Plasmon Mediated Strong Exciton-Photon Coupling in Semiconductor Nanocrystals. *Nano Lett.* **2010**, *10*, 274–278.
43. Fedutik, Y.; Temnov, V. V.; Schops, O.; Woggon, U.; Artemyev, M. V. Exciton-Plasmon-Photon Conversion in Plasmonic Nanostructures. *Phys. Rev. Lett.* **2007**, *99*, 136802.
44. Achermann, M. Exciton-Plasmon Interactions in Metal-Semiconductor Nanostructures. *J. Phys. Chem. Lett.* **2010**, *1*, 2837–2843.
45. Vasa, P.; Lienau, C. An Unusual Marriage: Coupling Molecular Excitons to Surface Plasmon Polaritons in Metal Nanostructures. *Angew. Chem., Int. Ed.* **2010**, *49*, 2476–2477.
46. Sugawara, Y.; Kelf, T. A.; Baumberg, J. J.; Abdelsalam, M. E.; Bartlett, P. N. Strong Coupling between Localized Plasmons and Organic Excitons in Metal Nanovoids. *Phys. Rev. Lett.* **2006**, *97*, 266808.
47. Schwartz, T.; Hutchison, J. A.; Genet, C.; Ebbesen, T. W. Reversible Switching of Ultrastrong Light-Molecule Coupling. *Phys. Rev. Lett.* **2011**, *106*, 196405.
48. Lienau, C.; Vasa, P.; Pomraenke, R.; Cirmi, G.; De Re, E.; Wang, W.; Schwieger, S.; Leipold, D.; Runge, E.; Cerullo, G. Ultrafast Manipulation of Strong Coupling in Metal-Molecular Aggregate Hybrid Nanostructures. *ACS Nano* **2010**, *4*, 7559–7565.
49. Lekeufack, D. D.; Brioude, A.; Coleman, A. W.; Miele, P.; Bellessa, J.; Zeng, L. D.; Stadelmann, P. Core-Shell Gold J-aggregate Nanoparticles for Highly Efficient Strong Coupling Applications. *Appl. Phys. Lett.* **2010**, *96*, 253107.
50. Fontcuberta-Morral, A.; Stellacci, F. Light-Matter Interactions: Ultrastrong Routes to New Chemistry. *Nat. Mater.* **2012**, *11*, 272–273.
51. Fofang, N. T.; Park, T. H.; Neumann, O.; Mirin, N. A.; Nordlander, P.; Halas, N. J. Plexcitonic Nanoparticles: Plasmon-Exciton Coupling in Nanoshell-J-Aggregate Complexes. *Nano Lett.* **2008**, *8*, 3481–3487.
52. Chen, H.; Shao, L.; Woo, K. C.; Wang, J.; Lin, H.-Q. Plasmonic–Molecular Resonance Coupling: Plasmonic Splitting *versus* Energy Transfer. *J. Phys. Chem. C* **2012**, *116*, 14088–14095.
53. Savasta, S.; Saija, R.; Ridolfo, A.; Di Stefano, O.; Denti, P.; Borghese, F. Nanopolaritons: Vacuum Rabi Splitting with a Single Quantum Dot in the Center of a Dimer Nanoantenna. *ACS Nano* **2010**, *4*, 6369–6376.
54. Schlather, A. E.; Large, N.; Urban, A. S.; Nordlander, P.; Halas, N. J. Near-Field Mediated Plexcitonic Coupling and Giant Rabi Splitting in Individual Metallic Dimers. *Nano Lett.* **2013**, *13*, 3281–3286.
55. Vasa, P.; Wang, W.; Pomraenke, R.; Lammers, M.; Maiuri, M.; Manzoni, C.; Cerullo, G.; Lienau, C. Real-Time Observation of Ultrafast Rabi Oscillations between Excitons and Plasmons in Metal Nanostructures with J-aggregates. *Nat. Photonics* **2013**, *7*, 128–132.
56. Dintinger, J.; Klein, S.; Bustos, F.; Barnes, W. L.; Ebbesen, T. W. Strong Coupling Between Surface Plasmon-Polaritons and Organic Molecules in Subwavelength Hole Arrays. *Phys. Rev. B* **2005**, *71*, 035424.
57. Berrier, A.; Cools, R.; Arnold, C.; Offermans, P.; Crego-Calama, M.; Brongersma, S. H.; Gomez-Rivas, J. Active Control of the Strong Coupling Regime between Porphyrin Excitons and Surface Plasmon Polaritons. *ACS Nano* **2011**, *5*, 6226–6232.
58. Hakala, T. K.; Toppari, J. J.; Kuzyk, A.; Pettersson, M.; Tikkanen, H.; Kunttu, H.; Torma, P. Vacuum Rabi Splitting and Strong-Coupling Dynamics for Surface-Plasmon Polaritons and Rhodamine 6G Molecules. *Phys. Rev. Lett.* **2009**, *103*, 053602.
59. Salomon, A.; Gordon, R. J.; Prior, Y.; Seideman, T.; Sukharev, M. Strong Coupling between Molecular Excited States and Surface Plasmon Modes of a Slit Array in a Thin Metal Film. *Phys. Rev. Lett.* **2012**, *109*, 073002.
60. Jackson, J. D. *Classical Electrodynamics*; Wiley: New York, 1962.
61. Bowden, C. M.; Dowling, J. P. Near-Dipole-Dipole Effects in Dense Media: Generalized Maxwell-Bloch Equations. *Phys. Rev. A* **1993**, *47*, 1247–1251.
62. Gray, S. K.; Kupka, T. Propagation of Light in Metallic Nanowire Arrays: Finite-Difference Time-Domain Studies of Silver Cylinders. *Phys. Rev. B* **2003**, *68*, 045415.
63. Taflove, A.; Hagness, S. C. *Computational Electrodynamics: The Finite-Difference Time-Domain Method*, 3rd ed.; Artech House: Boston, 2005.
64. Allen, L.; Eberly, J. H. *Optical Resonance and Two-Level Atoms*; Wiley: New York, 1975.
65. Sukharev, M.; Nitzan, A. Numerical Studies of the Interaction of an Atomic Sample with the Electromagnetic Field in Two Dimensions. *Phys. Rev. A* **2011**, *84*, 043802.
66. Garcia de Abajo, F. J. Colloquium: Light Scattering by Particle and Hole Arrays. *Rev. Mod. Phys.* **2007**, *79*, 1267–1290.
67. Bidégaray, B. Time Discretizations for Maxwell-Bloch Equations. *Numer. Methods Partial Differ. Equations* **2003**, *19*, 284–300.
68. Roden, J. A.; Gedney, S. D. Convolution PML (CPML): An Efficient FDTD Implementation of the CFS-PML for Arbitrary Media. *Microwave Opt. Technol. Lett.* **2000**, *27*, 334–339.